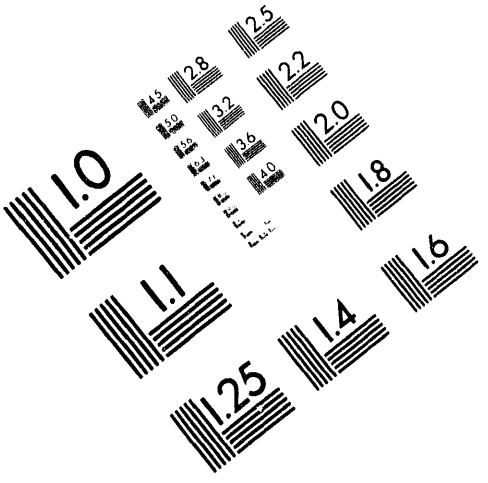

Association for Information and Image Management

1100 Wayne Avenue, Suite 1100
Silver Spring, Maryland 20910

301/587-8202

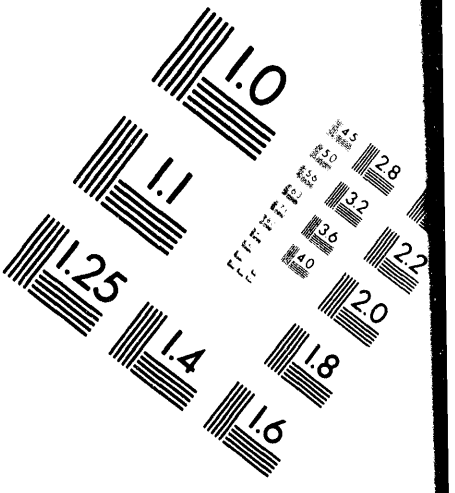

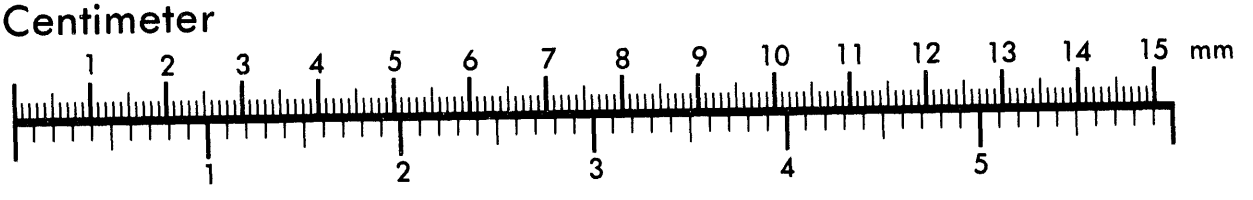

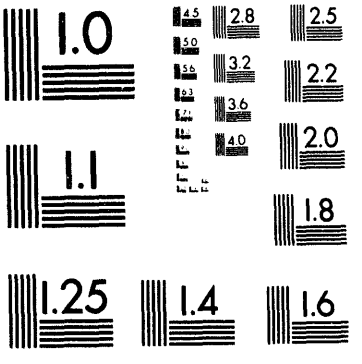

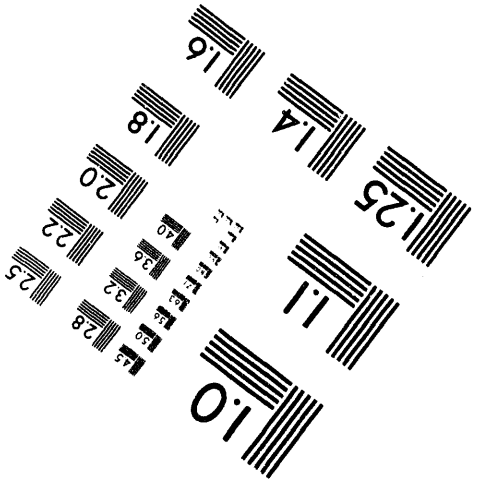

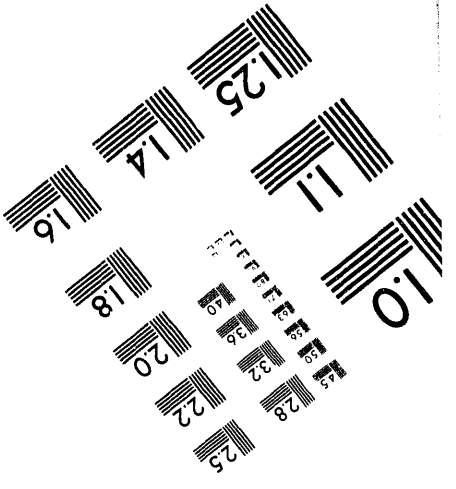

1 of 1

CONF-940135--7

The Effect of Fiber Coating Thickness on the Interfacial Properties of a Continuous Fiber Ceramic Matrix Composite

Edgar Lara-Curzio, Mattison K. Ferber and Richard A. Lowden
Metals and Ceramics Division
Oak Ridge National Laboratory
Oak Ridge, TN 37831-6064

ABSTRACT

The interfacial properties (coefficient of friction, residual clamping stress, residual axial stress, and debond stress) of a continuous fiber ceramic composite were determined by means of single-fiber push-out tests. The composite consisted of Nicalon™ fibers, that had been coated prior to matrix infiltration with carbon layers ranging in thickness from 0.03 to 1.2 μm, and a SiC matrix. It was found that the effective interfacial frictional stress decreased as the thickness of the carbon layer increased, from 24.6 ± 9.9 MPa for a thickness of 0.03 μm to 3.8 ± 1.4 MPa for a thickness of 1.25 μm. It was also found that both the coefficient of friction and the residual clamping stress decreased as the thickness of the carbon layer increased. These results are explained in terms of the state of residual stresses in this composite and the role of the fiber surface topography during fiber sliding.

INTRODUCTION

Because the strength and toughness of continuous fiber-reinforced ceramic composites (CFCCs) are significantly influenced by the forces acting at the fiber-matrix interface, substantial efforts have been dedicated in recent years towards the characterization of the interfaces and their properties in these materials. These efforts have included the development of experimental methods to determine both the interfacial shear strength and the sliding resistance between fiber and matrix, the formulation of analyses to model these tests, and the modification of interfaces to control the forces between the fibers and the matrix.

One approach of modifying the fiber-matrix interface in CFCCs consists in introducing interphases, which will alter not only the fiber bonding and sliding characteristics but would also protect the fibers during processing. To investigate and quantify the effect of fiber-matrix interphase thickness in the interfacial behavior of CFCCs, the interfacial properties of a model system with a range of fiber-matrix interphase thicknesses were determined by means of single-fiber push-out tests.

EXPERIMENTAL.

Material. The CFCCs studied were fabricated at the Oak Ridge National Laboratory by forced Chemical Vapor Infiltration (CVI) using a plain weave cloth of Nicalon™ fiber[1]. The fibers were desized and then coated with carbon and SiC using polypropylene and a mixture of methyltrichlorosilane and H_2, respectively. By controlling the time of residence of the fiber preform during carbon deposition, different fiber coating thicknesses ranging between 0.03 μm and 1.2 μm were obtained.

Sample Preparation. Rectangular specimens 8 x 3 x 2 mm where cut from the composite and embedded in metallographic epoxy to obtain wedged specimens, similar to the one depicted schematically in Figure 1. A specimen with wedged geometry is used because it provides an array of fiber embedded lengths. Samples were prepared following standard metallographic techniques that included polishing with 30, 15, and 6 μm diamond disks followed by 1 and 0.05 μm alumina slurry. The final dimensions of the wedged samples were 10 mm in diameter and 1 mm thick.

One potential disadvantage of using samples with woven fiber preforms for single-fiber push-out tests is that the fiber(s) of interest would not be oriented perpendicular to the sample surface. This problem is compounded when the fibers have non-circular cross sections. Therefore, special attention is paid throughout the sample preparation process to insure that the fibers considered are indeed perpendicular to the sample surface.

Test Procedure. Single fiber push-out tests were conducted using the Interfacial Test System (ITS). This apparatus was developed at the Oak Ridge National Laboratory (ORNL) as part of the DOE CFCC program and is currently available to industrial and university participants of the High Temperature Materials Laboratory User Program at ORNL. The system consists of a set of micropositioned X-Y-Z stages, an optical subsystem consisting of a TV camera and a high quality microscope, a load cell, a flat-bottomed diamond indentor 10 μm in diameter that is attached to the load cell, a capacitance gauge to determine the relative indentor displacement, and a personal computer for data acquisition and control. User intervention is only required to select the fibers that will be pushed. A schematic representation of the ITS is included in Figure 2 and a more detailed description of the apparatus and its operation can be found elsewhere [2].

The samples were mounted on a special sample holder using low melting temperature wax. The sample holder had a slot 0.75 mm wide and 10 mm long to allow fibers to protrude during push-out. Fiber loading was achieved at a constant displacement rate of 0.1 μm/sec by raising the sample against the fixed indenter using the Z-stage. Both the load and the sample surface displacement were sampled continuously during the test at a rate of 25 Hz.

RESULTS

Figure 3 shows a typical stress vs. fiber-end displacement curve for a SiC/SiC sample that had a fiber coating 0.1 μm thick. The stress was calculated as the ratio of the applied load and the fiber cross sectional area, while the fiber-end displacement was obtained from the difference between the total measured displacement and the contribution from the load train compliance. It has been found that the compliance of the load cell accounts for all of the load train compliance (4-5 μm/N), which was determined from the load vs. displacement curve obtained by loading the sample with a 500 μm diameter stainless steel rod. It should be noted that the shift in the stress vs. fiber-end displacement curve (Figure 3) after the load drop was artificially induced as a result of the load train compliance correction.

The stress vs. fiber-displacement curves exhibited a linear regime (A-B in Figure 3) up to point B that coincides with the start of fiber debonding. The occurrence of fiber debonding at the onset of non-linear behavior has been corroborated by progressively loading a fiber and visually examining the interface until debonding was observed. Furthermore, if the load is sampled fast enough, fiber debonding is usually accompanied by a small "jump" in the signal as indicated by point B in Figure 3. As the fiber continues to be pushed at a constant displacement rate, the load will continue to increase. The energy absorbed by the system will go to promote further debonding and to slide the debonded portion of the fiber against the matrix (or fiber coating)[1] in a process that is influenced by the fiber Poisson's effect.

The load eventually reached a maximum value (point D in Figure 3) when the debond length almost equals the original fiber embedded length. At this point the debond crack grows unstable and debonds the remaining portion of the fiber[2][3-4]. Since the load level maintained up to this point was necessary to promote fiber debonding and sliding, now that the fiber has been entirely debonded and pushed out, the system will require a lower stress

[1]For most of the samples with carbon coatings thicker than 0.3 μm, it was found that the fiber always debonded from and slid against the carbon interphase.

[2]In fact it has been argued that at the peak load the debond length is equal to the original embedded length minus 1.5 fiber radii[5].

level to continue sliding the fiber. In fact, this argument can be verified if we compare the magnitude of the load drop after pushout (D-E about 600 MPa) to that of the load required to initiate debonding (A-B about 610 MPa), as evidenced in Figure 3. The assumption that fiber pushout coincides with the drop of the load after this has reached a maximum value has been validated by studying the bottom of the sample before and after the peak load and corroborating that fiber protrusion occurs only after the load drop (Figure 4).

After pushout, the load attains a level necessary to continue sliding the fiber. An estimate for the interfacial shear stress can be obtained from this portion of the curve since

$$\bar{\tau} = \frac{\sigma r}{2 t} \quad (1)$$

where σ is the applied stress, t is the fiber embedded length, and r is the fiber radius. Because of size limitations of the indenter, the largest distance that a 15 μm fiber can be slid into the matrix is about 5 μm. Beyond this distance the indenter will hit the matrix (point G in Figure 3) and the load will start to climb again.

DATA ANALYSIS

Except for the portion of the stress vs. fiber-end displacement curve after push-out (E-G in Figure 3), from which it is possible to estimate the effective interfacial shear stress, it is difficult to infer anything else about the interfacial properties of composites from the experimental curves by themselves. Unfortunately some fibers are too small compared to the indentor dimensions, and, inevitably, the indentor will hit the matrix just after push-out, preventing the fiber from sliding over long distances. Recently a methodology was developed[6] to extract the composite interfacial parameters by fitting the progressive debonding and sliding portion of the stress vs. fiber-end displacement curve with the models of Hsueh[3] and Kerans & Parthasarathy[4]. It was also demonstrated that although the analytical forms of Hsueh's and Kerans & Parthasarathy stress-displacement relations are different, the predictions from both models are equivalent[6]. In this paper, the model of Hsueh was used to extract the interfacial parameters from the experimental push-out curves. According to this model, the relationship between the fiber-end displacement, u, and the applied axial stress, σ, is given by

$$u = \frac{h(\sigma+\sigma_d-2\sigma_z)}{2E_f} \quad (2)$$

where σ_d is the value of the stress required to initiate debonding, σ_z is the axial residual stress in the fiber and h is the sliding length. The sliding length and the interfacial shear stress will be given respectively by

$$h = \frac{r(\sigma_d - \sigma)}{2\tau} \quad (3)$$

$$\tau = -\mu(\sigma_c + \sigma_p) = -\bar{\tau} - \mu\sigma_p \quad (4)$$

where $\bar{\tau}$ is the intrinsic average shear stress and σ_p is the average contribution to the clamping stress due to Poisson's effect and is given as

$$\sigma_p = \frac{(\frac{\nu_f E_m}{E_f} - \frac{f\nu_m}{1-f})\sigma + (\frac{\nu_f E_m}{E_f} + \frac{f\nu_m}{1-f})\sigma_d}{2D} \quad (5)$$

where

$$D = \frac{1+f}{1-f} + \nu_m + \frac{(1-\nu_f)E_m}{E_f} \quad (6)$$

f is the fiber volume fraction, E refers to the elastic modulus, ν to Poisson's ratio and the subscripts f and m refer to the fiber and matrix respectively. Equation (2) is applicable when

$$\sigma_d \le \sigma \le \sigma_{pushout} \quad (7)$$

The assumptions leading to these relationships are: (1) the fiber is embedded in a large homogeneous medium; (2) σ_c arises only from the mismatch in the thermoelastic constants of the constituents, and (3) the fiber Poisson's effect is averaged along the debond length. Although the last assumption considerably simplifies the analysis, it does not degrade the capabilities of the model compared with the complete analysis[3].

The fitting of the experimental data with Hsueh's model[3] was accomplished by means of non-linear least squares techniques using (μ, σ_c, σ_z) as fitting parameters[6]. The fitting procedure is only restricted in the sense that the debond length must be slightly smaller than the fiber embedded length, which will limit the number of possible combinations of the fitting parameters .

Table I and Figures 5-7 summarize the results from the analysis. Table 1 includes the average values of the coefficient of friction, axial residual stress, debond stress, radial clamping stress, and interfacial shear stress. Figure 5 shows that the coefficient of friction decreased as the fiber coating thickness increased. Similarly it was found that the clamping residual stress σ_c decreased as the coating thickness was increased (Figure 6) . The combined effect of these two factors (i. e., $\bar{\tau} = \mu\sigma_c$) is a net decrease of the intrinsic interfacial shear stress as the thickness of the carbon coating increased (Figure 7). It must be pointed out that although large scatter was obtained for the values of μ or σ_c, the scatter in the values of $\bar{\tau}$ is comparably smaller. This fact is attributed in part to a property of Equation 2 for which several combinations of μ and σ_c would produce similar values of $\bar{\tau}$ and in turn similar stress vs. fiber-end displacement curves[6]. There was good agreement between the values of $\bar{\tau}$ obtained from fitting the debonding-progressive sliding portion of the stress vs. fiber-end displacement curves and those values obtained from the purely frictional portion of the curve (F-G in Figure 3), although this comparison could not be conducted for all tests for the reasons already given.

Likely sources for data scatter are the non-uniform fiber distribution in the composite and temperature variations during the composite fabrication. Figure 8 shows the in-plane von Mises stress contours in a typical composite and highlights the influence of neighboring fibers in the local states of stress. Although one advantage of single-fiber push-out over other interfacial tests (e. g. fiber pull-out, fragmentation) is that samples may be obtained from actual composite specimens, one disadvantage is that the condition specified by the model for an isolated fiber embedded in a homogeneous medium is not fulfilled when the fiber volume fraction is large.

DISCUSSION

In relation to the scatter in the values of μ and σ_c, a valid question that often arises is: which are the "true" values for μ and σ_c if many combinations of these two parameters would produce similar values for $\bar{\tau}$, and in turn, similar stress vs. fiber-end displacement curves?. One of the assumptions of Hsueh's model[3] was that σ_c results from the

mismatch in thermoelastic properties of the composite constituents. Therefore a thermoelastic analysis should give a good estimate of the "true" value of σ_c. Such an analysis for this particular composite system showed that the residual radial stress at the fiber-fiber coating interface decreases from -285 MPa to -218 MPa as the interphase thickness increases from 0.03 μm to 1.25 μm[3]. Although the values of the clamping stress as obtained from the application of Hsueh's model to the data were found to decrease as the interphase coating thickness increased, the magnitude of the change was found to be twice as large as that predicted from the thermoelastic analysis.

It has already been suggested that fiber surface roughness will contribute to the interfacial shear stress as the peaks on the fiber and matrix surface topographies overlap during fiber sliding[4]. Figure 9 shows a push-back test on this composites and the sitback in the curve (C) corroborates this argument. Other evidence of the role of fiber surface roughness on the interfacial behavior of CFCCs is given by the results in Figure 5. These results indicate that the coefficient of friction is largest for an interphase thickness comparable to the Nicalon™ fiber surface roughness which is of the order of a 30 nanometers for as-received fibers[8]. Because there is an order of magnitude difference between the stiffness of the SiC matrix and the radial stiffness of the carbon interphase, the roughness effects will become less pronounced as the thickness of the carbon interphase increases, as is suggested by the results. Studies are currently under way to quantify definitely the effect of fiber surface roughness on the interfacial properties of CFCCs by producing specimens with controlled degrees of fiber surface roughness.

CONCLUSIONS.

It was found by means of single-fiber pushout tests that the intrinsic interfacial shear stress $\bar{\tau}$ for a SiC(Nicalon™)/Graphite/SiC CFCC decreases as the fiber-matrix interphase layer thickness increases from 24.6 ± 9.9 MPa for a thickness of 0.03 μm to 3.8 ± 1.4 MPa for a coating thickness of 1.2 μm. It was also found that the coefficient of friction decreased as the coating thickness increased reaching a constant value of about 0.02 for carbon interphase thicknesses larger than 0.3 μm. For thinner coating sections, the effect of the fiber surface roughness is reflected in the coefficient of friction, since the mean average roughness of Nicalon™ fibers is about 30 nm and for fiber coating thicknesses of these dimensions the coefficient of friction was found to be highest. From a thermoelastic

[3]The thermoelastic analysis consists of a system of four concentric cylinders representing the fiber, the fiber coating, the matrix and a homogeneous medium with the effective properties of the composite. The analysis incorporated the transversely isotropic (θ-z) structure of the carbon interphase[7].

analysis it was estimated that the residual radial clamping stress decreases from -285 MPa to -218 MPa for coating thicknesses between 0.03 and 1.2 μm, and although the estimated σ_c obtained from the application of Hsueh's model to the push-out curves decreases with the carbon interphase thickness, but the magnitude of the change was twice as large as that estimated from the thermoelastic stresses. It is concluded that these differences arise in part from the contribution of fiber surface roughness to the clamping stress, from variations in processing conditions and from the effect of neighboring fibers in the local states of stress.

ACKNOWLEDGMENTS.

This work was sponsored by the US Department of Energy, Assistant Secretary for Conservation and Renewable Energy, Office of Industrial Technologies, Industrial Energy Efficiency Division, under contract DE-AC05-84OR21400 with Martin Marietta Energy Systems Inc. The authors are grateful to Stephan Russ for his dedication in the preparation of the samples, to Laura Riester for her work with the electron microscope and to H. T. Lin and Peter Tortorelli for reviewing the manuscript.

REFERENCES

1.- Bessmann, T., M., Sheldon, B., W., Lowden, R., A., and Stinton, D., P., "Chemical Vapor Infiltration," Science 253, September 6 (1991) 1104-09

2.- Wereszczak, A., A., Ferber, M., K., and Lowden, R., A., "Development of an Interfacial Test System for the Determination of Interfacial Properties in Fiber Reinforced Ceramic Composites," 13th. Annual Conf. Ceram. Comp, Cocoa Beach FL. January 1-17 (1993)

3.- Hsueh, C., H., "Interfacial Debonding and Fiber Pull-out Stresses of Fiber- Reinforced Composites: VII: Improved Analysis for Bonded Interfaces," *Matls. Sci. Eng.*, **A154** (1992) 125-32

4.- Kerans, R., J., and Parthasarathy, T., A., "Theoretical Analysis of the Fiber Pullout and Pushout Tests," *J. Am. Ceram. Soc.*, **74**, 7 (1991) 1585-96

5.- Liang, C., and Hutchinson, J., W., "Mechanics of the Fiber Pushout Test," *Mech. Mater*, **14** (1993) 207-21

6.- Lara-Curzio, E., and Ferber, M., K., "A Methodology for the Determination of the Interfacial Properties of Brittle Matrix Composites" submitted to *J. Matls. Sci* (1993)

7.- Lara-Curzio, E. Unpublished results. Oak Ridge National Laboratory (1993)

8.- K. L. More Oak Ridge National Laboraory. Private communication to E. Lara-Curzio (1993).

Interphase Thickness (μm)	μ	σ_c (MPa)	σ_z (MPa)	σ_d (MPa)	τ (MPa)
0.03	0.048 ± 0.03	-688 ± 378	-662 ± 223	-803 ± 315	24.61 ± 9.91
0.13	0.031 ± 0.014	-442 ± 174	-398 ± 87	-557 ± 160	11.9 ± 1.77
0.27	0.023 ± 0.03	-559 ± 428	-429 ± 354	-493 ± 313	3.85 ± 2.14
1.2	0.013 ± 0.01	-445 ± 222	-654 ± 254	-755 ± 272	3.83 ± 1.44

TABLE 1
Summary of Results

FIGURE CAPTIONS

Figure 1. Sample geometry used with the Interfacial Test System.

Figure 2.- Schematic representation of the Interfacial Test System.

Figure 3.- Stress vs. fiber-end displacement curve obtained from a single-fiber push-out test of a model CFCC (Nicalon™/C/SiC). The curve has been corrected by subtracting the contribution of the load train deformation from the total displacement. In the curve the following points are identified: (B) fiber debonding, (C) progressive debonding and sliding, (D) peak load followed by (E) push-out and (F) purely frictional sliding. The solid line is the best fit of the data using the model of Hsueh. The inset summarizes the results from the analysis.

Figure 4.- Electron micrograph showing fibers protruding from the sample bottom surface after push-out.

Figure 5.- Dependence of the coefficient of friction on the fiber coating thickness of a model CFCC (Nicalon™/C/SiC).

Figure 6.- Dependence of the clamping residual stress on the fiber coating thickness of a model CFCC (Nicalon™/C/SiC).

Figure 7.- Dependence of the effective interfacial shear stress on the fiber coating thickness of a model CFCC (Nicalon™/C/SiC).

Figure 8.a.- Cross sectional view of model CFCC.

Figure 8.b.- Finite element analysis of the cross sectional area of the composite in Figure 8.a. The stress field corresponds to the in-plane von Mises stress. These results demonstrate the influence of neighboring fibers in the local states of stress.

Figure 9.- Push-back test for a model CFCC (Nicalon™/C/SiC). The dip in the curve (C) indicates the fiber surface roughness does play a role in the fiber sliding behavior.

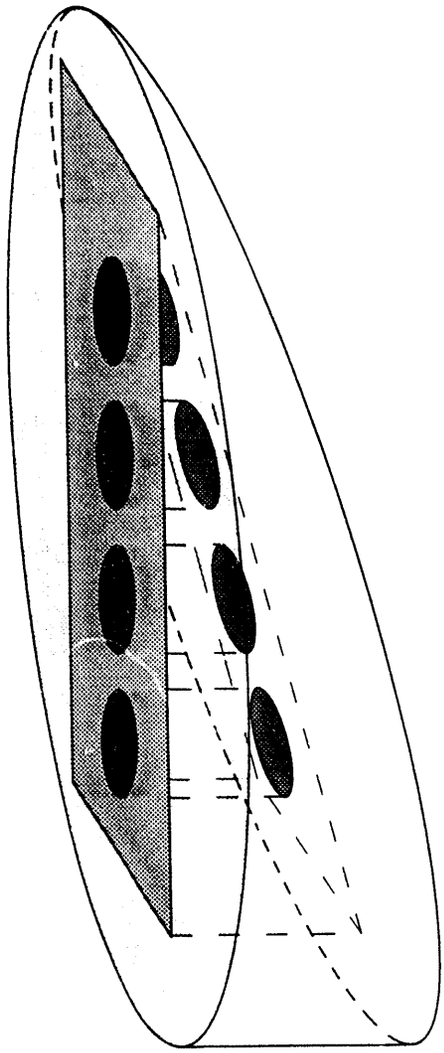

DISCLAIMER

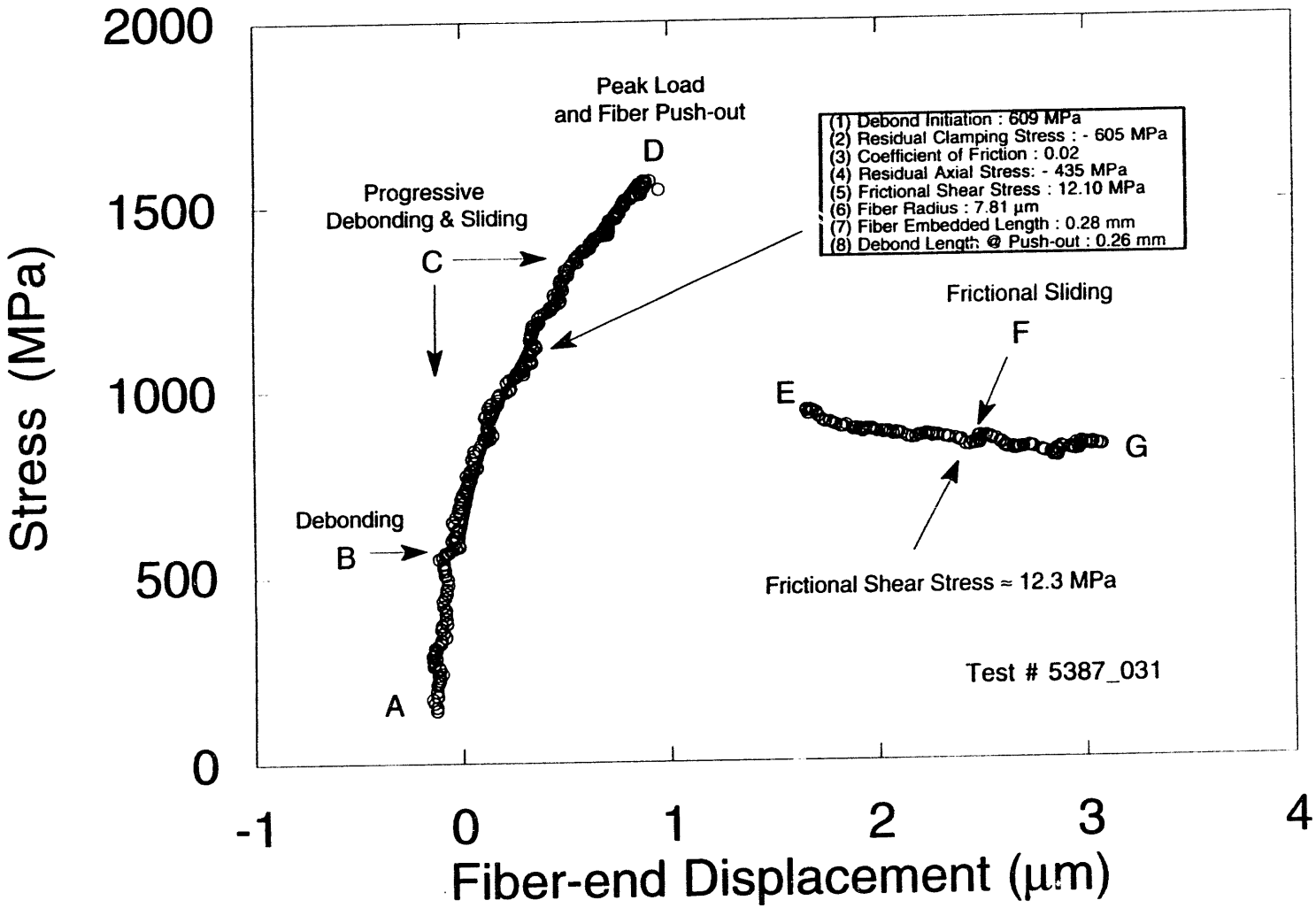
2000
1500
1000
500
0
Stress (MPa)
-1
0
1
2
3
4
Fiber-end Displacement (μm)
Peak Load
and Fiber Push-out
D
Progressive
Debonding & Sliding
C
Debonding
B
A
(1) Debond Initiation : 609 MPa
(2) Residual Clamping Stress : - 605 MPa
(3) Coefficient of Friction : 0.02
(4) Residual Axial Stress: - 435 MPa
(5) Frictional Shear Stress : 12.10 MPa
(6) Fiber Radius : 7.81 μm
(7) Fiber Embedded Length : 0.28 mm
(8) Debond Length @ Push-out : 0.26 mm
Frictional Sliding
F
E
G
Frictional Shear Stress ≈ 12.3 MPa
Test # 5387_031

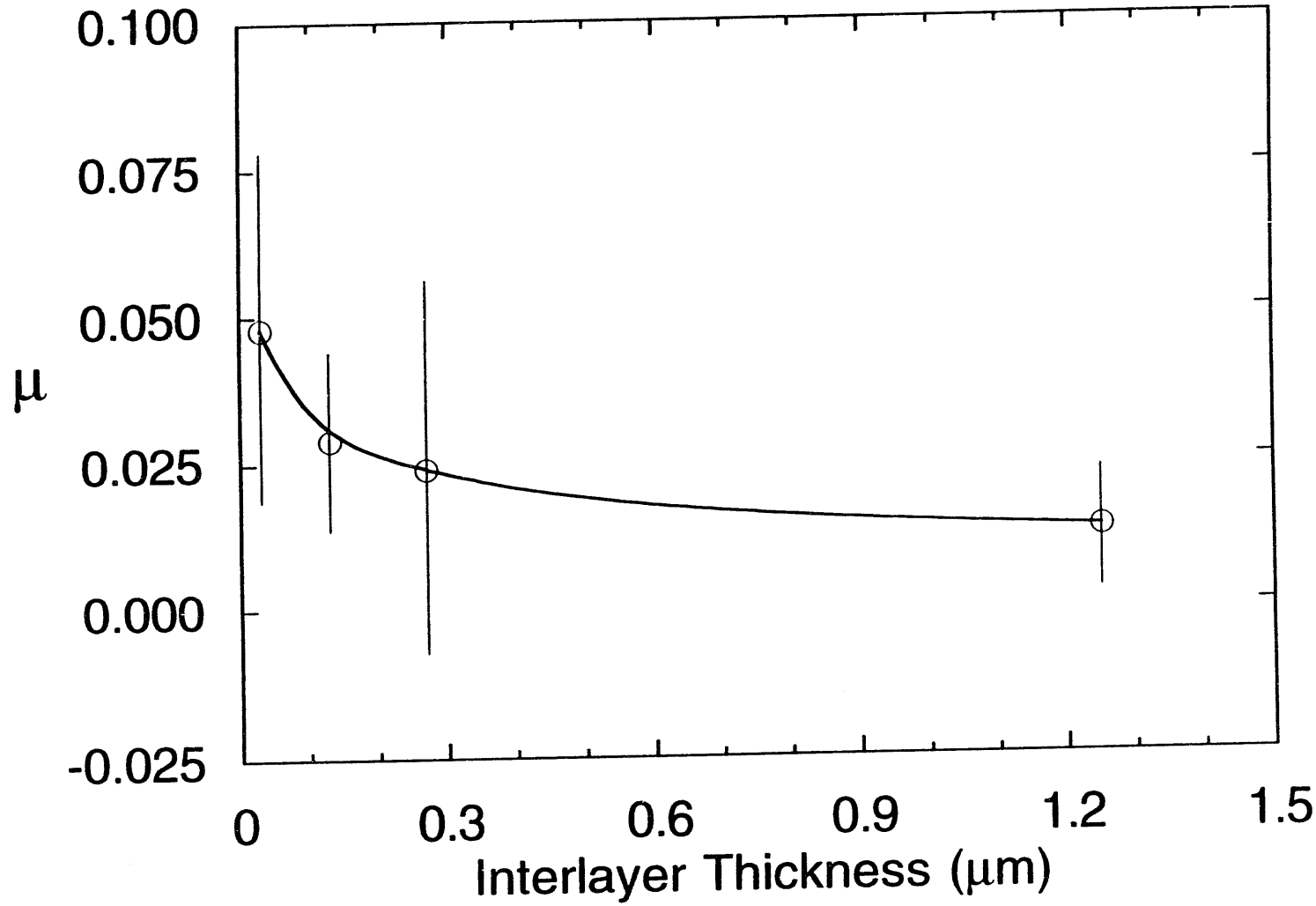
0.100
0.075
0.050
0.025
0.000
-0.025
μ
0
0.3
0.6
0.9
1.2
1.5
Interlayer Thickness (μm)

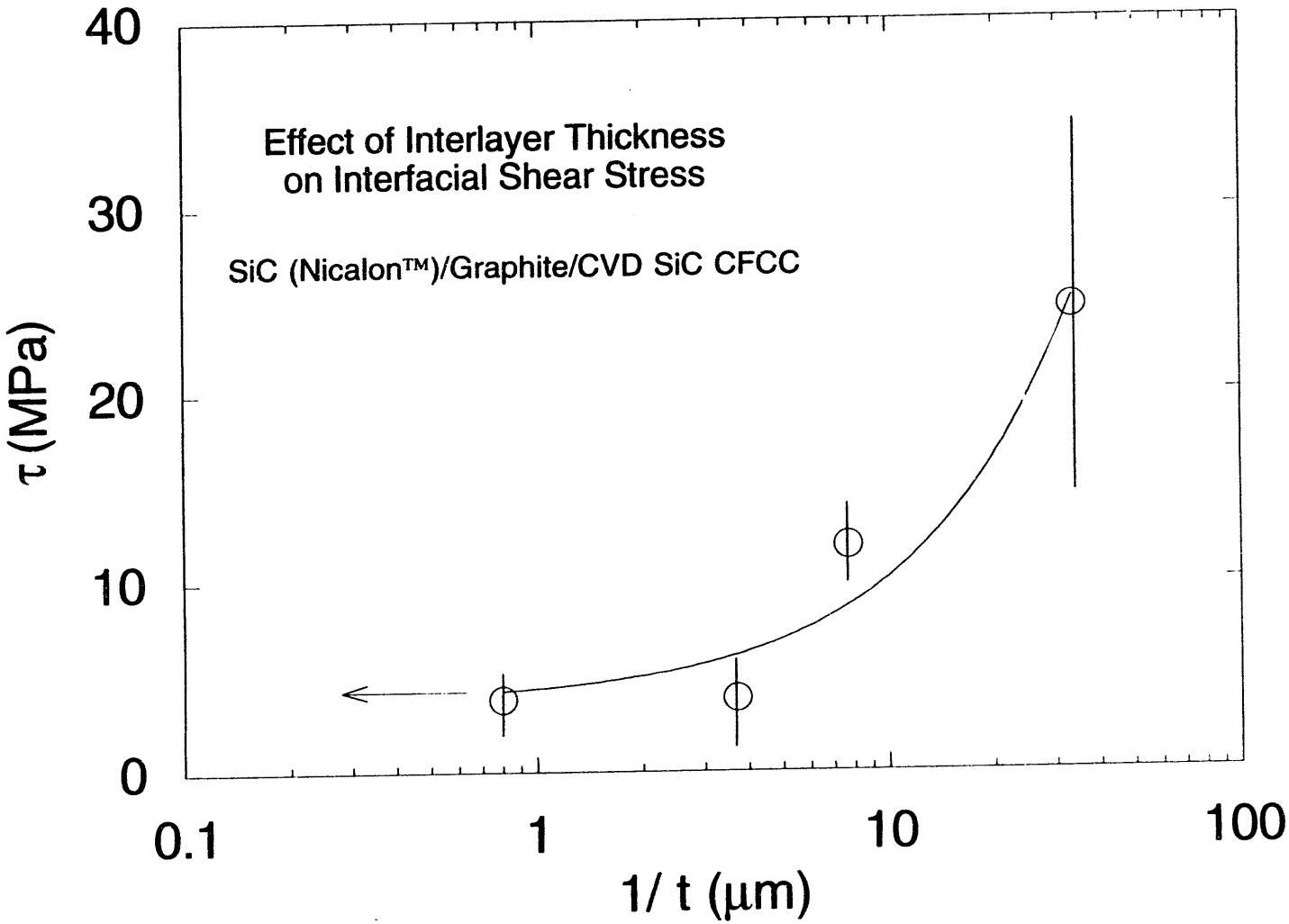
Effect of Interlayer Thickness
on Interfacial Shear Stress
SiC (Nicalon™)/Graphite/CVD SiC CFCC
τ (MPa)
40
30
20
10
0
0.1
1
10
100
1/ t (μm)

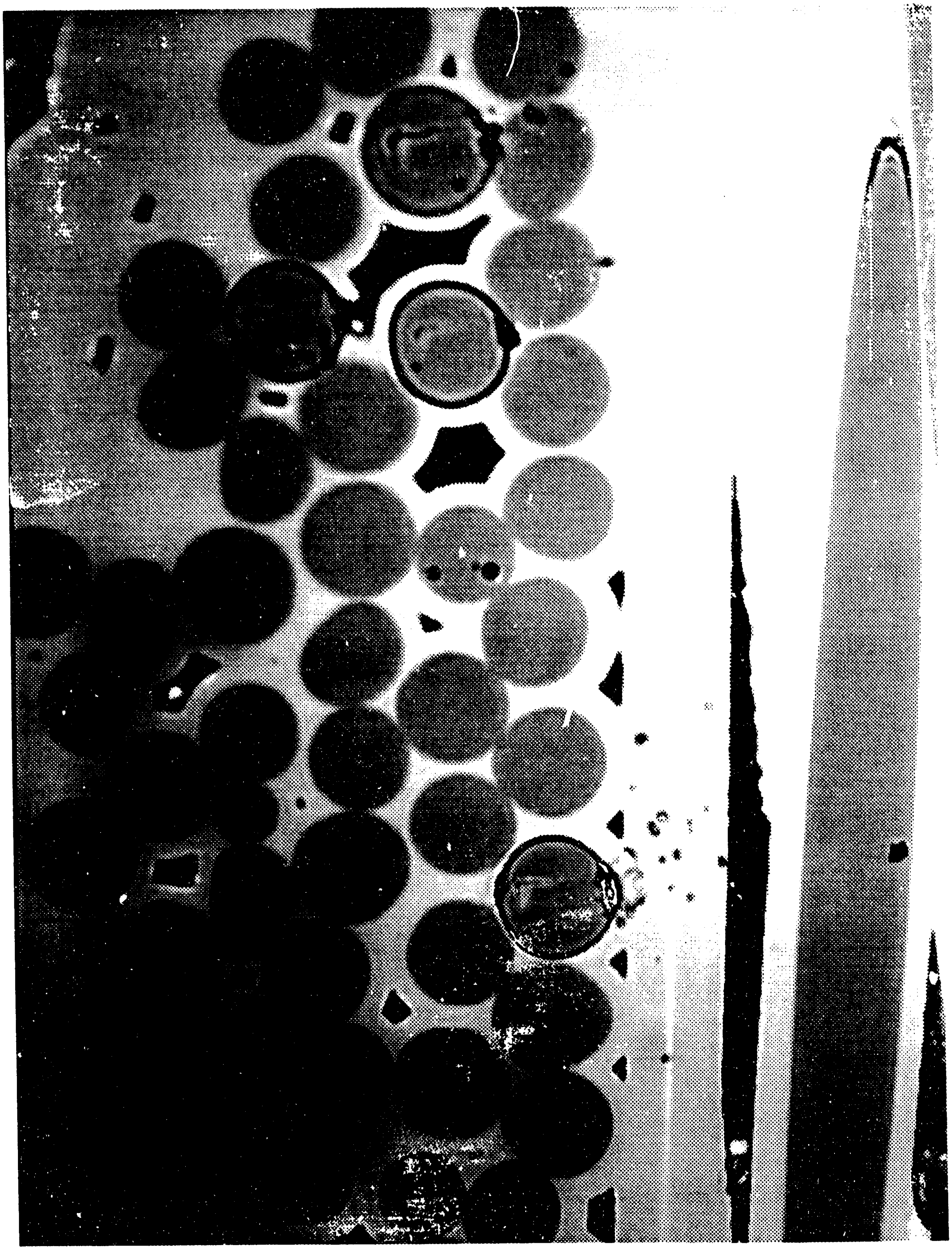

3.a

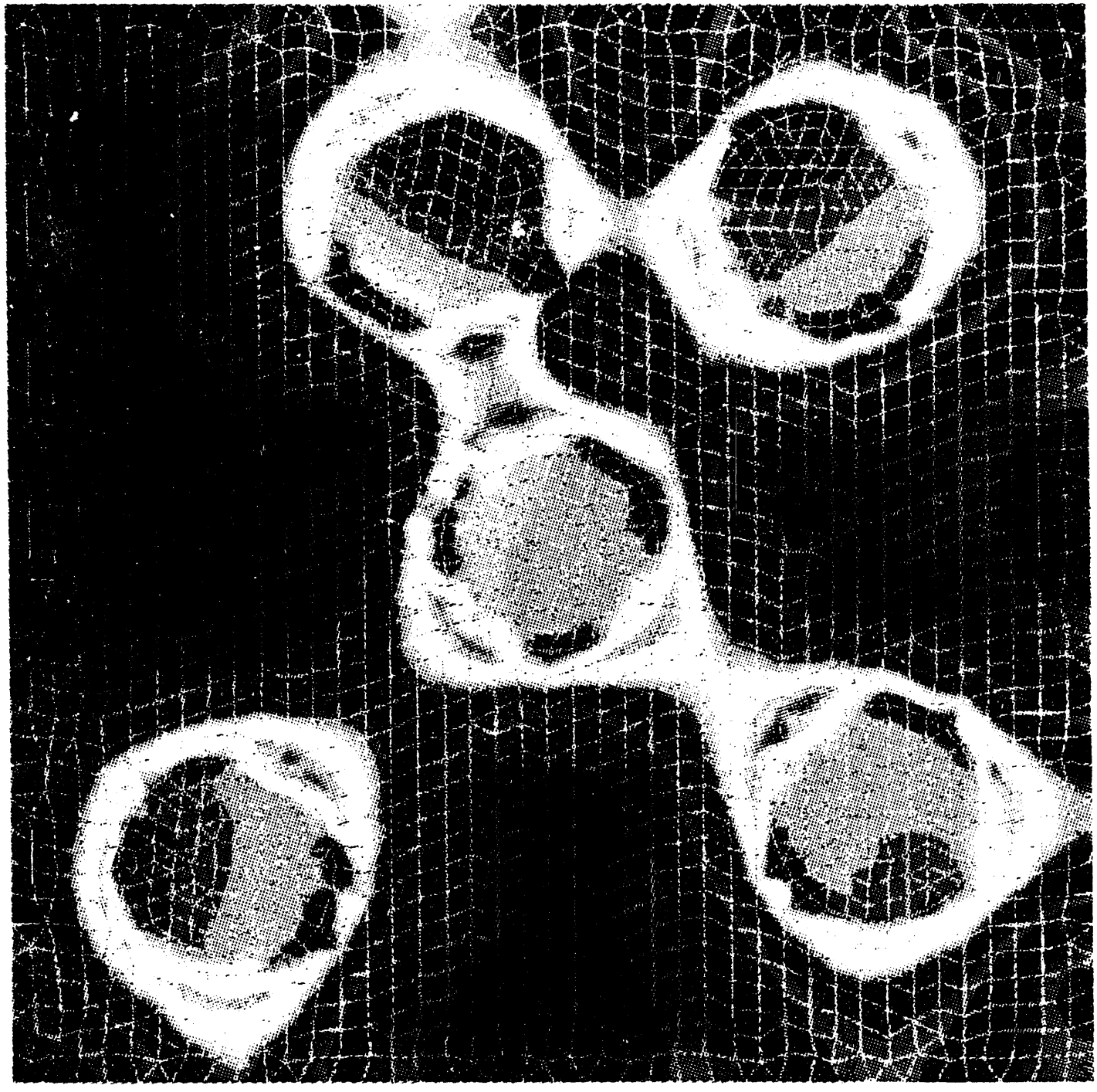

3.c

DATE
FILMED
10/17/94
END